Published in final edited form as:
Biochemistry. 2013 October 15; 52(41): 7305–7317. doi:10.1021/bi400576t.

First Three-Dimensional Structure of *Toxoplasma gondii* thymidylate synthase-dihydrofolate reductase: Insights for Catalysis, Interdomain Interactions, and Substrate Channeling

Hitesh Sharma[#a], **Mark J. Landau**[#a,b], **Melissa A. Vargo**[a], **Krasimir A. Spasov**[a], and **Karen S. Anderson**[a,b,*]

[a]The Department of Pharmacology, Yale University School of Medicine, New Haven, CT 06510

[b]The Department of Molecular Biophysics and Biochemistry, Yale University School of Medicine, New Haven, CT 06510

[#] These authors contributed equally to this work.

Abstract

Most species, such as humans, have monofunctional forms of thymidylate synthase (TS) and dihydrofolate reductase (DHFR) that are key folate metabolism enzymes making critical folate components required for DNA synthesis. In contrast, several parasitic protozoa, including *Toxoplasma gondii*, contain a unique bifunctional thymidylate synthase-dihydrofolate reductase (TS-DHFR) having the catalytic activities contained on a single polypeptide chain. The prevalence of *T. gondii* infection across the world, especially for those immunocompromised, underscores the need to understand TS-DHFR enzyme function and to find new avenues to exploit for the design of novel antiparasitic drugs. As a first step, we have solved the first three-dimensional structures of *T. gondii* TS-DHFR at 3.7 Å and of a loop truncated TS-DHFR, removing several flexible surface loops in the DHFR domain, improving resolution to 2.2 Å. Distinct structural features of the TS-DHFR homodimer include a junctional region containing a kinked crossover helix between the DHFR domains of the two adjacent monomers, a long linker connecting the TS and DHFR domains, and a DHFR domain that is positively charged. The roles of these unique structural features were probed by site-directed mutagenesis coupled with pre-steady state and steady state kinetics. Mutational analysis of the crossover helix region combined with kinetic characterization established the importance of this region not only in DHFR catalysis but also in modulating the distal TS activity, suggesting a role for TS-DHFR interdomain interactions. Additional kinetic studies revealed that substrate channeling occurs in which dihydrofolate is directly transferred from the TS to DHFR active site without entering bulk solution. The crystal structure suggests that the positively charged DHFR domain governs this electrostatically mediated movement of dihydrofolate, preventing release from the enzyme. Taken together, these structural and kinetic studies reveal unique, functional regions on the *T. gondii* TS-DHFR enzyme that may targeted for inhibition, thus paving the way for designing species specific inhibitors.

[*]To whom correspondence may be addressed. Phone: (203)-785-4526; karen.anderson@yale.edu Karen Anderson Yale University School of Medicine, Department of Pharmacology 333 Cedar St., Rm SHM B350 New Haven, CT 06511.

Data deposition: The atomic coordinates have been deposited in the Protein Data Bank, www.pdb.org (PDB ID codes 4EIL for loop truncated and 4ECK for WT TS-DHFR).

Supporting Information Available

Supporting information consists of fifteen supplementary images with additional figures detailing *T. gondii* TS-DHFR structure and kinetics. This material is available free of charge via the Internet at http://pubs.acs.org

Keywords

thymidylate synthase; dihydrofolate reductase; transient kinetics; toxoplasmosis; domain communication; substrate channeling

Introduction

For most organisms folate metabolism and nucleotide synthesis are linked via the activities of dihydrofolate reductase (DHFR) and thymidylate synthase (TS).[1, 2] TS catalyzes the formation of the nucleotide deoxythymidine monophosphate (dTMP) from deoxyuridine monophosphate (dUMP) with the aid of (6R)-L-5,10-methylene-tetrahydrofolate (CH_2H_4F), which is converted to dihydrofolate (H_2F) upon the transfer of one carbon unit.[3, 4] DHFR on the other hand converts the H_2F to tetrahydrofolate (H_4F) through a hydride transfer step utilizing the co-factor NADPH (Fig. 1A).[5] While these enzymes are expressed on separate polypeptides in almost all other organisms including humans, in the opportunistic parasites Toxoplasma gondii, Leishmania major, Cryptosporidium hominis, Trypansoma cruzi, Babesia bovis and *Plasmodium falciparum*, TS and DHFR are linked together to form a bifunctional enzyme (Fig. 1B).[3, 6-10] It has been suggested that bifunctional forms of TS-DHFR might exhibit "substrate channeling," which is defined as the transfer of a metabolite from one enzyme active site to another without allowing diffusion of the molecule into bulk solution.[11-13] In this scenario, dihydrofolate is directly transferred from the TS site to the DHFR site (Fig. 1A). Substrate channeling has been suggested to play an integral role in numerous essential cellular functions, have implications for an understanding of metabolic regulation, and in this instance, offer a survival advantage for the parasite.[11]

As illustrated in Figure 1B, the overall domain architecture among the bifunctional TS-DHFRs differs substantially for individual parasites. Some such as *L. major* and *P. falciparum* contain an N-terminal extension of the DHFR (shown in yellow, Fig. 1B) whereas others such as *C. hominis*, *T. gondii*, and *P. falciparum* contain a junctional region between the DHFR and TS (shown in green, Fig. 1B). An overall sequence alignment for the TS and DHFR from human and the bifunctional forms of TS-DHFR[#] shows that TS is rather highly conserved while DHFR is more variable (Supporting Information, Fig. S3).[7, 14]

The first crystal structure solved for a bifunctional TS-DHFR was that of *L. major* (Lm) [6]. This structure, complexed with TS and DHFR active site inhibitors, revealed a homodimer in which each monomer of the enzyme contains an N-terminal DHFR domain that rests on the shoulders of the TS domain.[6, 7, 15] In the Lm structure, the TS domain forms the majority of the dimerization interface while the DHFR domains are spatially separated. This has also been shown to be the case for *T. cruzi* (Tc). [(8)] More recent structures for those bifunctional enzymes containing a junctional region where the TS and the DHFR domains of each monomer are linked together [*C. hominis* (Ch), *B. bovis* (Bb), and *P. falciparum* (Pf)] show distinct structural differences. In contrast to the Lm structure, the structures of bifunctional enzymes with a junctional region show that DHFR domains from each monomer are closer together and a part of this junctional region forms a crossover or "donated" helix that interacts with the catalytic B-helix of the DHFR domain adjacent monomer.[6-10] These key differences between the bifunctional TS-DHFR enzymes from various parasitic species have lead to their classification of Class I or Class II in which the presence of the junctional region defines Class I, while its absence defines Class II.[7, 16]

[#]TS-DHFR, thymidylate synthase-dihydrofolate reductase is a functional designation as catalysis at TS precedes catalysis at DHFR; elsewhere the bifunctional enzyme is called DHFR-TS based on a genetic classification as DHFR domain is located N-terminal to TS.

In the current work, we describe the first crystal structure of the bifunctional TS-DHFR enzyme from *T. gondii* as a new member of the Class I family that contains several structural features unique to this parasite. The functional importance of these features was examined with mutational analysis and kinetic characterization. Additional structural and kinetic studies establish the substrate channeling of dihydrofolate from the TS to the DHFR sites as well as provide an understanding of how this process may be mediated at a structural level. The availability of the structure also suggests several novel strategies that could be exploited for the design of species specific inhibitors.

Materials and Methods

Chemicals

All buffers and other reagents employed were of the highest commercial purity. 7,8-Dihydrofolate (H_2F) was chemically prepared by the reduction of folic acid (Sigma) with sodium hydrosulfite.[17] Tritium-labeled and unlabeled CH_2H_4F were synthesized as previously described using tritiated or unlabeled folic acid, respectively, as starting material, as previously described.[18] NADPH was purchased from Sigma and dUMP from MP Biomedicals. The propargyl dideazfolate (PDDF) used in the studies were generously provided by Dr. Roy Kisliuk and Dr. Ann Jackman.

Purification of T. gondii TS-DHFR

T. gondii TS-DHFR was prepared from *E. coli* BL21 cells (Invitrogen) freshly transformed with PET15b plasmid containing the coding sequence for *T. gondii* TS-DHFR. The *T. gondii* TS-DHFR plasmid was a generous gift from Dr. David S. Roos. For the single amino acid mutations, site-directed mutagenesis was performed using a QuikChange mutagenesis kit (Stratagene). For the loop truncations (residues deleted: 49-73 and 201-219) and crossover helix deletion (residues 291-296), 5'-phosphorylated primers (IDT) flanking the region to be deleted were used in PCR, the resulting product then ligated together with T4 DNA ligase (New England Biolabs) to delete the specific portion of the loops.

The protein was purified using an affinity column of methotrexate bound to agarose (Sigma), as described previously.[19, 20] A PD-10 column (Amersham Biosciences) was also used to remove residual H_2F after purification. The concentration of purified *T. gondii* TS-DHFR was determined by spectrophotometrically at 280 nm, using an extinction coefficient of 71,850 $M^{-`1}cm^{-1}$. The enzyme was flash frozen in storage buffer 25 mM Tris 7.3, 10 mM DTT, and 10 % glycerol and stored in −80 °C.

Steady state kinetic experiments

Steady state TS and DHFR kinetic experiments were performed by incubating 100 nM of enzyme with a saturating concentration of one TS or DHFR ligand (100 μM, confirmed to be well above saturating) and measuring the reaction rate at varying concentrations of the complementary TS or DHFR ligand (up to 250 μM). Experiments were performed in 1X enzyme buffer: 50 mM Tris pH 7.8, 25 mM $MgCl_2$, 1 mM EDTA, 2 mM DTT. The DHFR activity was measured by a decrease in absorbance at 340 nm as NADPH and H_2F were converted to $NADP^+$ and H_4F ($\Delta\varepsilon = 10\ mM^{-1}cm^{=1}$). The TS activity was measured by an increase in absorbance at 340 nm as dUMP and CH_2H_4F were converted to dTMP and H_2F ($\Delta\varepsilon = 6.4\ mM^{-1}cm^{=1}$). Rate constants for steady state experiments were estimated by fitting the data to a Michaelis-Menten hyperbolic curve ($v = V_{max}[S]/(K_m+[S])$, where v is the reaction rate, [S] the concentration of substrate, and K_m the Michaelis constant) using the curve-fitting program, Kaleidagraph (version 4.03, Synergy Software).

Stopped-flow kinetic experiments

Stopped-flow experiments were performed using a Kintek SF-2001 apparatus (Kintek Instruments, Austin, TX). To the determine rate of the DHFR reaction, coenzyme fluorescence resonance energy transfer experiments were carried out with 290 nm excitation and emission using an interference filter at 450 nm. Concentrations of enzyme and substrates described are those after mixing. To find the single turnover rate (k_{chem}) of the DHFR reaction, enzyme (50 μM in 2X enzyme buffer: 100 mM Tris pH 7.8, 50 mM $MgCl_2$, 2 mM EDTA, 2 mM DTT) was incubated with NADPH (250 μM) and then mixed with H_2F (25 μM). Changes in fluorescence upon mixing were monitored and the resultant data were fit in Kaleidagraph to a single exponential curve, *Fluorescence* = $Ae^{(-kchem*time)}$, where A is the amplitude of fluorescence and k_{chem} is the exponential rate constant. Stopped-flow traces were smoothed using the Kintek software smoothing program which averages together adjacent points to reduce noise.

For the TS burst reaction, enzyme (25 μM) was preincubated with excess dUMP (1 mM) and mixed with excess CH_2H_4F (500 μM). Changes in absorbance at 340 nm were monitored, and the trace was fit to a burst curve *Fluorescence* = $Ae^{(-kburst*time)} + k_{ss}$*time, where where A is the amplitude of absorbance, k_{burst} is the exponential phase rate constant and k_{ss} is the linear phase rate constant.

Rapid Chemical Quench

The bifunctional TS-DHFR reaction was measured via using a Kintek RFQ-3 Rapid Chemical Quench Apparatus (Kintek Instruments, Austin, TX). The reactions were initiated by mixing 15 μL enzyme solution (enzyme + 2X enzyme buffer) with 15 μL radiolabeled CH_2-H_4F. The reactions were terminated by quenching with 89 μL of a solution of 0.78 N KOH, 10% sodium-ascorbate, and 200 mM 2-mercaptoethanol. The TS-DHFR single turnover bifunctional reaction was monitored by addition of [^{3}H]-CH_2H_4F (10 μM) to enzyme (50 μM), dUMP (500 μM), and NADPH (500 μM). For the pulse-chase experiment, 50 μM of enzyme was incubated with 500 μM dUMP and 500 μM NADPH. The reaction was initiated by mixing the enzyme solution with 25 μM of [^{3}H]-CH_2H_4F and 150 μM unlabeled H_2F. The data from the single enzyme turnover experiments were fit to a single exponential equation using Kaleidagraph.

High Performance Liquid Chromatography (HPLC) Analysis

Tritiated products of the rapid chemical quench experiments were quantified by HPLC in combination with a radioactivity flow detector as described previously.[18, 21] The HPLC separation was performed using a BDS-Hypersil C18 reverse phase column (Thermo) with a flow rate of 1 ml/min. An isocratic separation using a solvent system of 10% methanol in 200 mM triethylammonium bicarbonate at pH 8.0 was used. The elution times were as follows: H_4F, 9 min; H_2F, 18 min; CH_2H_4F, 20 min.

Crystallization

Crystals of the WT and the loop truncation mutant *T. gondii* TS-DHFR were obtained by vapor diffusion when protein (10 mg/mL) in storage buffer, active site ligands dUMP and NADPH (10 mM each), and active site inhibitors (2S)-2-[(4-{[(2,4-diaminopteridin-6-yl)methyl](methyl)amino}phenyl)formamido]pentanedioic acid (methotrexate) and N^{10}-propargyl-5,8-dideazafolate (PDDF) (10 mM each) were mixed with 18% PEG 3350, 0.1 M potassium formate in a 1:1 ratio. The crystals grew within 4–6 days and were stabilized in a solution containing an increased amount of PEG 3350. They were then cryoprotected in two steps with stabilizing solutions containing 15 and 25% ethylene glycol, and flash-frozen in liquid nitrogen.

Structure Determination

Diffraction data for the WT and the loop truncation mutant *T. gondii* TS-DHFR were collected at the beam line station, X25 at the National Synchrotron Light Source at Brookhaven National Laboratory (Upton, NY). Initial processing and scaling of the raw data were carried out by using HKL2000.[22] General handling of scaled data were done in CCP4[23] and corrected for anisotropy.[24] There were four dimer molecules per asymmetic unit with the majority of contacts made between the DHFR domain of one dimer and the TS of the other.

Initial phases were obtained by molecular replacement with PHASER[25] in CCP4 by using *C. hominis* TS (PDB ID 1QZF) and *Pneumocystis carinii* DHFR (PDB ID 3OAF) as search models.[7, 16, 26] These domains (not including the linker) were used as a search model to reduce model bias in this part of the structure. The model of the WT *T. gondii* TS-DHFR was built by using the program COOT.[27] The crystal structure of the loop truncation mutant was solved by molecular replacement using the model of the WT *T. gondii* TS-DHFR as the search model. Refinement was carried out by using REFMAC with TLS (translation, libration, and screw rotation parameters) and restrained refinements. During refinement, electron density was observed for the crossover helical region and part of the linker. (See additional details provided in Supporting Information and Supplementary Figures 1 and 2 including sim omit (F_o-F_c) difference density map of the crossover helix). The side chain density for W296 was used as the starting point for this stage of the model building, and eventually the junctional region was linked to the TS domain belonging to the same polypeptide chain. There is some missing density. The model for residues from 254-287 that lie in the portion between the junctional region and the DHFR domain could not be built because little or no electron density was observed for this portion of the molecule. For WT, the final R_{cryst} was 34.66% and the final R_{free} was 39.86% (Table 1). The loop truncated mutant refined to an R_{cryst} of 22.44% and an R_{free} of 24.55%. Figures were generated using the program Pymol.[28]

Results

The crystal structure of the *T. gondii* (Tg) TS-DHFR presented here reveals it belongs to Class I and has several unique structural features that may influence various aspects of catalytic function (Fig. 2). The closest structural homolog to Tg TS-DHFR is that for Ch TS-DHFR.[7] The *T. gondii* DHFR domain contains three flexible surface loops that are not present in the structure of *C. hominis* (Ch). The WT Tg TS-DHFR crystals diffracted to 3.7 Å and removal of two of these loops in a loop truncated Tg TS-DHFR improved resolution to 2.2 Å (Table 1) without impacting catalytic activity. While the structures of the Class I bifunctional TS-DHFR enzymes all contain a crossover helix within the junctional region, this helical segment varies in length and amino acid composition. The crossover helix is in an extended helical conformation in all other Class I structures, including Ch TS-DHFR. However, in the structure of Tg TS-DHFR, this helix is kinked due to the presence of a proline residue and makes a fewer number interactions with the DHFR domain of the other monomer as does the crossover helix of Ch TS-DHFR (Fig. 2B, Table 2). Mutational analysis of this kinked crossover helix in Tg TS-DHFR coupled with pre-steady state and steady state kinetics were employed to identify possible roles of this region in governing catalytic function. Further kinetic studies examined whether substrate channeling was operative in the transfer of dihydrofolate from active site of TS where it is formed to the DHFR site where it is converted to tetrahydrofolate.

I. Structural Analysis of Toxoplasma gondii TS-DHFR

The overall structure—The initial WT Tg TS-DHFR structure was solved to 3.7 Å. Structural analysis and sequence alignment (Fig. S3) show that the *T. gondii* DHFR domain in the bifunctional Tg TS-DHFR is larger than the homologous one in *C. hominis* due to three flexible surface loops. The first of these loops consists of ~30 residues located between the B-helix and the third β-strand. The second loop consists of ~20 residues located between third β-strand and the D-helix, and the third of the largest loops is ~25 residues in length located near the C-terminus of each DHFR domain. When Loops 1 and 3 were deleted (residues 49-73 and 201-219, respectivly), crystals diffracted to 2.2 Å. The structures of WT and the loop truncated version were nearly identical (RMSD of 0.19 Å) as expected (Table 1). Kinetic analysis comparing the WT and loop truncated forms of Tg TS-DHFR shows that catalytic function is not affected (Tables 3 and 4).

Based on structural comparisons and sequence alignment with TS and DHFR from other monofunctional and bifunctional versions of the enzymes, the DHFR domain of Tg TS-DHFR is 252 residues, the TS domain 289 residues, and the junctional region is 69 residues providing a monomer (Fig. 1B) that has a molecular mass of 69 kilodaltons. [14] The Tg TS-DHFR structure is a homodimer as illustrated in Figure 2A. In each monomer, the N-terminal DHFR domain (residues 1-252) and the larger C-terminal TS domain (residues 322-610) are tethered together through the junctional linker region, ~69 residues in length, a portion of which interacts with the DHFR domain of the other monomer through a kinked crossover helix. This crossover helix is kinked due to proline 292, limiting the number of residues that interact with the catalytic helix of the DHFR domain relative to the crossover helix of other Class I TS-DHFRs (Fig. 2B). Residues 253 to 284 located between the crossover helix in one monomer and the DHFR domain of the adjacent monomer exhibit little or no electron density, indicating that this portion of the molecule is disordered (Fig. 2A). The TS and DHFR active sites were defined by the presence of active site ligands (Fig. 2A, ligands shown in yellow). The TS active site was denoted by the substrate, dUMP, and a TS folate inhibitor, PDDF (N^{10}-propargyl 5,8-dideazafolate) while the DHFR active site was defined by the substrate, NADPH, and a DHFR folate inhibitor, methotrexate (MTX). The distance between the TS and DHFR active sites on the same monomer is ~44 Å as measured through the enzyme between the TS and DHFR folate ligands, PDDF and methotrexate. The active site of the TS in the Tg TS-DHFR is located in an orthogonal position relative to the DHFR active site which is on the opposite side of the same monomer. The distance from the active site TS of the Tg TS-DHFR to the active site of the DHFR located on the same face of the adjacent monomer is ~75 Å. Similar active orientations between the TS and DHFR have been observed for Ch and Pf TS-DHFR.[7, 10] This is in contrast to Lm TS-DHFR where the TS and DHFR active sites are on the same face of the monomer.[6]

The combined surface area for the DHFR/TS interface (including canonical TS, DHFR, and junctional region) is ~1800 $Å^2$ (per monomer, calculated from solvent accessible surface area). As illustrated in the ligand plot (Fig. S4), the interactions between the TS and the DHFR domains within the same monomer are comprised of both electrostatic and hydrophobic interactions (summarized in Table 2) that are predominately hydrophobic. These include hydrophobic contacts between F231, F319, and M297 as well as P242, I573, and V596. In the TS-DHFR homodimer, while interactions between the DHFR domains exist through the junctional region, interactions between TS domains from each monomer form the majority of the dimerization interface similar to the other bifunctional TS-DHFR enzymes.

The DHFR domain—The overall fold of the *T. gondii* DHFR domain resembles other DHFR structures containing a central twisted β-sheet formed from 8 β-strands, 7 of which are parallel and one that is anti-parallel as well as four α-helices, including the catalytic B helix. There are also 3 flanking β strands and another α-helix (Fig. S5A). As illustrated in this figure, an overlay of the Tg DHFR (blue) and the Ch DHFR (orange), reveals these two species have similar DHFR domains.

The electron density for DHFR active ligands, methotrexate and NADPH, was apparent in the initial maps (Fig. S5B). A view of the DHFR active site shows bound ligands and highlights key protein-ligand interactions (shown in magenta, Fig. S5C). A comprehensive view of protein-ligand interactions for MTX and NADPH is shown in the ligand plots (Fig. S6 A-B) and summarized in Table 2. These residues include D31, F32, F35, L94, and R97 that interact with MTX. In the *T. gondii* DHFR domain, the catalytic helix contains a nonconserved F32 and a conserved F35 that make stacking interactions with the pteridine ring of the active site folate analog methotrexate.[20, 29] Residues interacting with the substrate NADPH included the conserved residues A10, I17, R81, T83, S103, and G153 and the nonconserved residue A154. The Tg DHFR domain also contains a conserved tryptophan, W25, in the "M20" loop (Fig. S5A).[29] This is a dynamic loop found in other DHFR species whose conformations are thought to be involved in shielding the active site from solvent during catalysis.[20, 29] While the overall fold is similar for the Tg and Ch DHFR domains, there are key differences between these two species most of which can be attributed to differences in loop lengths that decorate the surface of the DHFR domain.

The *T. gondii* DHFR domain of the bifunctional enzyme consists of 252 residues from the N-terminus to the start of the junctional region, while the *C. hominis* DHFR domain consists of 179 (Fig. 1B). The larger size of the Tg DHFR domain compared with Ch DHFR domain is primarily due to larger loops between the β-strands and the α-helices. The most N-terminal loop in the Tg DHFR domain consists of ~33 residues spanning from T41 to F74, and of only ~9 residues from N41 to N50 in the *C. hominis* TS-DHFR. In the *T. gondii* TS-DHFR crystal structure, however, most of this region is disordered. The second loop spans residues 103-124 in *T. gondii* and residues S76 to V88 in *C. hominis* contributing to a difference of ~9 residues. This second loop is fairly well ordered compared to the other two larger loops. The last loop spans residues ~184-227 in the *T. gondii* TS-DHFR corresponding to loop residues 148-155 in the TS-DHFR from *C. hominis*. In this last loop, residues 196-219 of the model could not be built in the *T. gondii* TS-DHFR due to a lack of electron density in this region. As expected these loops do not change the overall fold of the domain's core.[20, 29]

TS domains—The TS domain of Tg TS-DHFR forms the largest portion of the dimerization interface mainly through a five-stranded β-sheet from each monomer (Fig. 2A). The interactions between these two β-sheets places the active sites of each TS domain away from the dimerization interface. By comparing the overall fold of the *T. gondii* TS with that of the *C. hominis*, it can be shown that the domain is structurally conserved with RMSD of ~2.7 Å. In addition to sharing an overall structural homology, the domain also contains conserved residues that are the hallmark of TS.[3] The structure also reveals that the *T. gondii* TS domain is only 2 residues larger than the one in *C. hominis* (Fig. 1B), therefore supporting predictions from primary sequence alignment indicating that this domain is more structurally conserved than the DHFR domains.[7]

A conserved histidine (322 in *T. gondii*) marks the N-terminus of the domain and a catalytic cysteine (489 in *T. gondii*) is responsible for catalysis. Well-defined electron density for the TS ligands, dUMP and the folate analog, PDDF establish the active site (data not shown). As observed for the TS in other species including Ch TS, the active site for Tg TS is

comprised of residues from both monomers. The nucleophilic C489 interacts with the dUMP to anchor this substrate as a covalent complex. The residues involved in binding the TS ligands, dUMP and PDDF are shown in the ligand plots (Supplemental Fig. 7A-B) and summarized in Table 2. These include several conserved arginines that bind dUMP (R344, R510 as well as R469 and R470 from the adjacent monomer). Residues are involved in binding the folate analog PDDF include I402, D513, L516, F520, as well as the nonconserved R603 and conserved M608 located on the C-terminal tail of the TS-domain. Previous kinetic studies evaluating TS catalysis for ChTS and Tg TS have shown that the rate of catalysis for the *C. hominis* is almost 10-fold higher compared with *T. gondii*.[30, 31] Sequence alignment between the two species (Figure S1) shows that Tg TS contains a conserved phenylalanine (F374) and glycine (G377) whereas these two residues in Ch TS (A287) and (S290) are not conserved. Structural insight for these differences between the two species is provided by superimposing the active sites and examining the TS active ligands, dUMP and PDDF. As illustrated in Supplemental Figure S8, the position of the dUMP substrate relative to the folate ligand, PDDF is shifted for Tg (Fig. S8, shown in red) relative to Ch (Fig. S8, shown in green). In this comparison, it is apparent that the distance between the C5 of dUMP and CP1 of the PDDF folate ligand involved in methyl transfer has increased 1 Å for Tg relative to Ch. In addition, S290 (Ch) and G377 (Tg) show the largest differences in atomic coordinates and the position of the glutamyl tail of the PDDF folate substrate analog was altered. Also, the catalytic rate of the TgTS is significantly slower (>10-fold) relative to ChTS.[30, 31]

These correlative structural and kinetic findings are consistent with our previous results examining the structure and kinetics of a Ch TS mutant in which the S290 was mutated to a glycine (S290G) similar to that found in the Tg TS. In the case of the S290G Ch mutant, the catalytic TS rate was reduced over 10-fold, the distance between the atoms involved in methyl transfer (C5 of dUMP and CP1 of PDDF) was increased 1.2 Å, and the position glutamyl tail of PDDF was different. Taken together, these data suggest that interactions with PDDF's glutamyl tail may be necessary for correct placement of ligands in the active site, thus explaining the observed differences in TS catalytic activity between the two species.

Junctional region—In the *T. gondii* TS-DHFR, the DHFR and the TS domains are connected by a linker composed of ~69 amino acids (Fig. 2A). The Fo-Fc omit maps for WT and loop truncated mutant TS-DHFR (Fig. S1 and S2) both revealed clear continuous electron density showing helicity indicated the presence of the crossover helix. Determining the location of W296 in the crossover helix was facilitated by considering that this residue might be in a similar location as F207 in *C. hominis* as suggested by sequence alignment (Fig. S1-S3). The crystal structure for *C. hominis* TS-DHFR shows that F207 packs into a hydrophobic pocket formed by the DHFR domain's catalytic B-helix.[7] In the *C. hominis* TS-DHFR, F207 is located near the C-terminus of the crossover helix and fits into the hydrophobic pocket that is formed by F172, F163, Y170, and F35.[7] In the *T. gondii* TS-DHFR, a hydrophobic cavity is formed by the residues F245, F236, Y243, and H34 that enables interactions with W296 (Fig. 2C).

The crossover helix in the junctional region of *T. gondii* TS-DHFR (Fig. 2B) (291-APVLAW-296)differs significantly in its composition from the crossover helices in either *P. falciparum* (283-DDEEEDDFVYFNF-295) or *C. hominis* (194-KSIDDTVDLLGEIF-207).[7, 10, 16] The portion of the crossover helix that interacts with the DHFR domain is 6 residues in length in *T. gondii*, less than half of the length of either *P. falciparum* (13 residues) or *C. hominis* (14 residues). This is due to P292 that kinks it away from the DHFR domain (Fig. 2B, C). Also, unlike the numerous acidic residues on the crossover helices from *P. falciparum* and *C. hominis*, the crossover helix from *T. gondii* is

completely aliphatic. This is illustrated in the ligand plot showing the interactions between the crossover of one DHFR domain in one monomer and the catalytic B-helix of the adjacent monomer (Fig. S9).

II. Probing Catalysis and Interdomain Interactions

The structural analysis of the *T. gondii* TS-DHFR reveals a unique feature, a kinked crossover helix (Fig. 2B), that may have a functional role in governing TS and DHFR catalysis and interdomain interactions. The role of the crossover helix was examined by mutational analysis coupled with detailed kinetic characterization. A combination of steady state and transient kinetic analysis was employed to assess functional effects of mutations in crossover helix of the Tg TS-DHFR bifunctional enzyme.

Effects of crossover helix mutations on DHFR activity—A series of three mutant forms of Tg TS-DHFR were designed and prepared to examine the role of crossover helix in catalysis. The first mutant in Tg TS-DHFR was designed to understand the role of the kink in the crossover helix. This kink is due to the helix breaking properties of proline 292 (Fig. 2B). The P292A mutant was made to determine the effects of a straightened helix on DHFR activity. The W296A and helix deletion (residues 291-296, Δ-helix) mutants were constructed to determine the significance of the anchoring and the presence of the crossover helix, respectively.

Steady state kinetic analysis determined the effects of these three crossover helix mutations on DHFR activity through the measurements of the K_m of the ligands and the overall rate of catalysis (k_{cat}), (Fig. S10A-B). These experiments revealed that the P292A mutation weakened the K_m for the active site ligand H_2F by approximately 6-fold and NADPH by less than two fold (Table 3). The W296A and Δ-helix mutants had a more pronounced effect on substrate binding. The K_m for NADPH of the W296A mutant was approximately 4-fold weaker, and about 6-fold weaker for the Δ-helix mutant. The W296A mutation weakened the K_m of H_2F by about 100-fold, whereas the Δ-helix mutation weakened it about 40-fold. As illustrated in Table 3, none of these mutations had an impact on the k_{cat} which reflects the rate of product release, previously established as the rate limiting step of the DHFR reaction.[31] As illustrated in Supplemental Figure S10C, the P292A, helix deletion, and W296A mutants substantially reduced the DHFR catalytic efficiency for using H_2F as a substrate by approximately 7-fold, 30-fold, and 100-fold, respectively. Shown in Table 3 are the steady state kinetic constants for the loop truncated form of Tg TS-DHFR, demonstrating that its kinetic behavior is similar to that of WT.

While steady state kinetic analysis allows an initial assessment of kinetic behavior, a transient kinetic analysis provides the opportunity to establish the kinetic pathway directly and examine individual steps including chemical catalysis. One type of transient kinetic experiment examines a single enzyme turnover in which enzyme is used in excess over substrate. A single enzyme turnover experiment is particularly informative to examine chemical catalysis since product formation is not rate limiting.

Single turnover turnover experiments were used to directly measure the rate of DHFR chemistry (k_{chem}) (Fig. 3, Fig. S11, Table 3). The crossover helix mutations were made to determine their effects on the rate of hydride transfer by monitoring the decrease in NADPH fluorescence to determine the rate of chemistry (k_{chem}) for WT and the three mutants. These experiments revealed that the W296A (Fig. 3B) and helix deletion (Fig. S11B) mutations reduced the k_{chem} approximately four-fold compared to that of the WT (Fig. 3A). On the other hand, the k_{chem} of the P292A (Fig. S11A) straightened helix was almost two-fold greater than that of WT. The loop truncated mutant had a k_{chem} for DHFR that was 75% that of WT.

Taken together, these kinetic analyses show that the crossover helix plays an important in modulating DHFR catalysis as well as proper positioning/orientation of substrates at the DHFR active site. These effects are likely mediated by interdomain interactions between crossover helix within the DHFR domain of one monomer and key contacts with the adjacent DHFR monomer.

Effects of crossover helix mutations on TS activity—Crossover helical contacts that involve DHFR interdomain interactions are important for optimal DHFR function and were negatively impacted by two of the crossover helix mutants, W296 and the helix deletion. Previous studies with the *L. major* TS-DHFR suggested TS-DHFR interdomain communication important for catalytic activity.[32] Therefore, these two crossover helix mutants were examined further to probe for distal effects on TS catalysis. Unlike the DHFR reaction where k_{cat} reflects the rate limiting step of product release, the k_{cat} of the TS reaction reflects the rate limiting step of chemistry where the methylene group of CH_2H_4F is transferred to dUMP to form dTMP and H_4F.[31] To determine the K_m of dUMP and CH_2H_4F, WT and mutant forms of TS-DHFR were incubated with a saturating concentration of CH_2H_4F and the reaction was initiated with varying concentrations of dUMP. Both of the W296A and Δ-helix mutations weakened the K_m of dUMP approximately 5-fold compared to that of WT but had little effect on the K_m of CH_2H_4F (Fig. S12 A-B, Table 4). The Δ-helix mutation had little or no effect on the k_{cat} while the W296A mutation reduced it by approximately one half. As illustrated in Supplemental Figure S12C, each of these mutations had a significant effect on the TS catalytic efficiency for utilizing dUMP as a substrate.

Additional transient kinetic analysis was carried out to compare the pre-steady state burst rate, reflective of the non-rate limiting isomerization step,[31] for the WT and the crossover helix mutants W296A and Δ-helix (Fig. S11C). Both of the mutations decreased the k_{burst} by a factor of 2 (Table 4). Collectively, the results from pre-steady state and steady state experiments provide evidence that the crossover helix impacts both TS catalytic activity and substrate positioning/orientation (Table 4). These effects are likely mediated by TS-DHFR interdomain interactions.

III. Evidence for substrate channeling in bifunctional Tg TS-DHFR

As illustrated in Figure 1A, it has been suggested the bifunctional *T. gondii* TS-DHFR enzyme may exhibit substrate channeling of dihydrofolate from the TS active site to that of DHFR without release into bulk solution.[33] It is notable that previous kinetic studies suggest that *C. hominis* TS-DHFR, the closest structural homolog, does not exhibit channeling behavior[21] whereas *P. falciparum* TS-DHFR, which has a similar structure, and *L. major* TS-DHFR, which has quite a different structure, each show evidence of substrate channeling. [32, 34]

To test this question in Tg TS-DHFR, a pulse-chase experiment with the TS-DHFR bifunctional single turnover reaction involving the conversion of radiolabeled (denoted by *) $*CH_2H_4F$ to $*H_2F$ at the TS active site and $*H_2F$ to $*H_4F$ at the DHFR site was performed. As illustrated in the experimental design in Scheme 1, if *T. gondii* TS-DHFR were able to channel, the presence of cold H_2F in solution would be expected to have a minimal effect on the bifunctional reaction (Scheme 1A). However, if the enzyme did not channel, radiolabeled H_2F would be able to freely diffuse into solution after being produced by the TS reaction (Scheme 1B). The excess cold H_2F in solution would therefore be able to out-compete the H_2F produced by the TS for the H_2F binding sites in the DHFR domain. A substantial buildup of radioactive H_2F and a decrease in the apparent rate of radiolabeled H_4F production would therefore be expected.

A comparison of a pulse-chase experiment using the Tg TS-DHFR and Ch TS-DHFR is shown in Figure 4. The time course for the conversion of $*CH_2H_4F$ to $*H_2F$ at the TS active site and $*H_2F$ to $*H_4F$ at the DHFR site for the Tg TS-DHFR is shown in Figure 4A. Despite the presence of a six-fold excess of unlabeled H_2F, no significant buildup of radiolabeled H_2F was detected, indicating that the enzyme did not release radiolabeled H_2F into bulk solution (Fig. 4A). Absorbance data confirmed the presence of a large amount of unlabeled H_2F still in solution, verifying that the DHFR active site of the Tg TS-DHFR enzyme had a preference for the $*H_2F$ produced by the TS reaction. When this experiment was performed using the Ch TS-DHFR, a large buildup of $*H_2F$ was detected before a significant formation of $*H_4F$ occurred (Fig. 4B, red arrow) consistent with previous findings.[21] For the Tg TS-DHFR, the rate of $*CH_2H_4F$ consumption ($3.2 \pm 0.4\ s^{-1}$) and $*H_4F$ production ($3.1 \pm 0.5\ s^{-1}$), were approximately equal, indicating no lag between the two reactions. On the other hand, for Ch TS-DHFR, the rate of $*H_4F$ production ($2.8 \pm 0.8\ s^{-1}$) was substantially slower that the rate of $*CH_2H_4F$ consumption ($14.1 \pm 5.5\ s^{-1}$) indicating a lag due to dissociation $*H_2F$ into bulk solution and rebinding to the enzyme at the DHFR active site.

To further probe the molecular mechanism of the distinct differences in substrate channeling behavior between Tg TS-DHFR and Ch TS-DHFR, mutants that were impaired in TS and/or DHFR activity were examined. It might be suggested that the presence of channeling in *T. gondii* and the absence in *C. hominis* TS-DHFR might be due to differences the ratio of catalytic rates of the TS and DHFR enzymes rather than by actual channeling of dihydrofolate. The DHFR k_{chem} for Tg TS-DHFR is approximately three- to four-fold faster than that Ch TS-DHFR whereas Ch TS-DHFR has an unusually fast TS reaction due to the presence of non-conserved residues at the TS active site.[35] A fast TS rate could lead to a buildup of H_2F and conversely, a slower rate of DHFR catalysis would require more time to bind and be converted to product leading to an apparent lag time between the two reactions. Therefore, the buildup of H_2F for Ch TS-DHFR in the bifunctional reaction might be due to a fast TS rate of chemistry and a slower rate of DHFR catalysis. Our previous studies have shown that a point mutant of Ch TS-DHFR, S290G, substantially slows the rate of TS catalysis without impacting DHFR rate.[30, 35] Mutational analysis of the Tg TS-DHFR in the current study has shown that mutations in the crossover helix, W296A and helix deletion, slow the DHFR catalysis to rates similar to Ch TS-DHFR. Additional pulse-chase single enzyme turnover experiments were carried out with the Ch S290G TS-DHFR mutant and the W296A and helix deletion Tg DHFR mutants and the ratio of dihydrofolate to tetrahydrofolate was determined at the peak concentration of dihydrofolate to quantify the amount of buildup. As illustrated in Supplemental Figure S13, none of the crossover helix mutants generated a larger amount of buildup relative to that WT Tg TS-DHFR (ratio ~0.5). In WT Ch TS-DHFR however the peak ratio was ~5 and similar for the Ch TS-DHFR S290G mutant ~3. This mutational probing of substrate channeling suggests that a rapid rate of TS catalysis does not explain the buildup of H_2F in Ch TS-DHFR and the lack of channeling is causing the higher ratio of H_2F:H_4F. Moreover, the crossover helix mutants of Tg TS-DHFR that have slower rates of DHFR catalysis, similar to Ch TS-DHFR, do not buildup H_2F and maintain their kinetic channeling behavior. Taken together, these studies make a compelling kinetic case for substrate channeling in *T. gondii* TS-DHFR.

The underlying structural features that might govern whether each species exhibits substrate channeling were also considered. It is notable, for instance, that while Tg TS-DHFR does shown substrate channeling, the species closest in structure, Ch TS-DHFR, does not. To examine whether there might be species differences in surface charge distribution, the structures were evaluated. As illustrated in Figure 5 (A-D), a comparison of the coulombic surface charge distribution of *L. major*, *P. falciparum*, and *T. gondii* to *C. hominis* TS-DHFR revealed that the *C. hominis* was the only species to contain a strongly negatively-

charged DHFR domain. The negative charge could result in the dissociation of dihydrofolate into bulk solution explaining the lack of channeling behavior in *C. hominis* TS-DHFR. A representation of the electrostatic field lines for each species (Fig. S14), indicates that the negatively charged dihydrofolate would be directed to the more positively charged DHFR domain for *L. major*, *T. gondii*, and *P. falciparum* (not shown) while the negatively charged DHFR domain for *C. hominis* would likely facilitate dissociation of the H_2F into bulk solution.

Discussion

In this report, the first three-dimensional structure of the *T. gondii* TS-DHFR is presented along with insights into catalysis, interdomain communication, and substrate channeling.

The structure of Tg TS-DHFR homodimer revealed a unique kinked crossover helix within the junctional linker between TS and DHFR monomer that contacts the DHFR domain of the adjacent monomer. The crossover helix is primarily aliphatic in nature and interactions with the neighboring DHFR domain are mediated by hydrophobic residues. A summary of electrostatic and hydrophobic interactions between the crossover helix and the adjacent DHFR domain are listed in Table 2. As shown in Table 2, a number of these interactions are hydrophobic, including W296. The helical composition and kink due to the presence of proline 292 are not observed in other protozoal bifunctional TS-DHFR species. Mutational analysis and kinetic characterization allowed the functional role of the crossover helix to be established.

The kinetic analysis of *T. gondii* TS-DHFR suggests that proper anchoring of the crossover helix by W296 is responsible for ligand binding and catalysis at both catalytic sites. If the crossover helix is deleted or changes its position due to the W296A mutation, the position of catalytic B-helix residues could be altered leading to changes in substrate binding, and therefore in the rates of chemistry and substrate release.

Steady state experiments of the crossover helix mutations suggest that the helix helps DHFR domain obtain a correct tertiary structure since these mutations affect the K_m. The kinked crossover helix helps stabilize binding in steady state analysis while a straightened one increases the k_{chem} of the DHFR under pre-steady state conditions. Despite its distal location from the TS active site, the crossover helix is also able to modulate the binding of dUMP and impact both the steady state and burst rates of the TS reaction.

The structure offers some clues for how these interdomain allosteric interactions may be mediated. The electrostatic and hydrophobic protein-protein interactions between the TS and DHFR domains are summarized in Table 2. The structure reveals that residues in the linker region downstream of the crossover helix interact directly with the TS domain. As illustrated in Supplemental Figure S15, a zoomed view of the crossover helix and the TS active site highlights some of the key structural elements that may be involved in mediating communication and residues that may be involved (shown in yellow). Hydrophobic residues in the crossover helix, including I290, interact with F319. Phenylalanine 319 is located in a turn between the linker and the start of the TS domain. Also located in this turn region is H316 that is involved in a salt bridge with E567. Glutamate 567 is also located in an area that lacks secondary structure, however it links to a helix (residues 556-565) which is further connected to the C-terminal tail that covers the TS active site. The lower part of this helix is also linked to a loop near the TS active site. It is possible that the interaction between H316 and E567 may be disrupted when the position of the crossover helix is altered through mutation. The loss of this interaction might in turn effect the position of helix (556-565) and also alter the adjoining loop and C-terminal tail which are important in modulating catalysis

at the TS active site. An overall change in the position of the crossover helix may alter the interactions between the linker and the TS domain thus abolishing the key interactions necessary for optimal catalysis.

Previous studies[33] as well as the current detailed kinetic analysis and pulse-chase experiments offer convincing evidence for subtrate channeling of dihydrofolate from the TS to the DHFR active sites in *T. gondii* TS-DHFR. Similar kinetic analyses support substrate channeling in bifunctional forms of *L. major* and *P. falciparum* TS-DHFR[12, 32, 34] but not in *C. hominis* TS-DHFR.[21] These observations pose the questions of the underlying structural features for each enzyme and possible general facets of the structure that might govern channeling behavior.

As illustrated in the domain comparisons in Figure 1B, each bifunctional enzyme has unique structural regions that could confer distinct properties in governing enzyme catalysis, interdomain interactions, and substrate channeling. Previous mutational analysis coupled with kinetic characterization of bifunctional TS-DHFR from *L. major, P. falciparum*, and *C. hominis* and the current study of *T. gondii* have defined how of these structural features from each species may play a role in modulating TS and DHFR catalysis and interdomain interactions.[21, 32, 36, 37] These structural features, however, were not responsible for the differences observed in substrate channeling behavior for each species. Therefore, a closer look at the structures was taken with an emphasis on Ch TS-DHFR and Tg TS-DHFR as they are close structural homologs. Earlier studies have suggested a potential role for surface charges in the transfer of the negatively charged dihydrofolate from the TS to the DHFR active site.[6] It might be hypothesized that a positively charged surface would facilitate the transfer of dihydrofolate to the DHFR site. A comparison of the amino acid sequences for the TS-DHFR from *T. gondii* (GenBank accession code: AAB00163) and *C. hominis* (GenBank accession code: 1QZF_A) revealed a difference in the overall number of positive charges in the DHFR domains. The Tg TS-DHFR and Ch TS-DHFR have a similar number of negative charges, (Glu or Asp), 25 versus 28 respectively. However Tg TS-DHFR has 15 more positivie charges (Lys, Arg, or His) than that of C. hominis, 33 versus 18.

Most important, however, is the distribution of these charges on the surface of the enzyme between the TS and DHFR domains. Based on an electrostatic surface respresentation for the structure of *L. major*, a continuous “electrostatic highway” of positive charges was suggested that involved specific lysine and arginine residues that might play a role in a “handing-off” mechanism mediated by conformational changes to serve as a conduit for transfer of dihyrofolate from the TS to the DHFR site.[6, 33] Previous modeling of electrostatic isopotential contours in *L. major* and *P. falciparum* revealed a continuous region of positive electrostatic potential connecting the TS and DHFR active sites.[38, 39] However, the comparisons of the crystal structures of *T. gondii, C. hominis*, and *P. falciparum* TS-DHFR, suggests that a continuous pathway of charges is not well defined (Fig. S14). Moreover, mutational analysis with the *L. major* targeting these specific lysines and arginines did not affect substrate channeling.[36] Accordingly, a positive electrostatic pathway alone may not be sufficient for channeling and suggests that the prominent negative charges on the surface of the *C. hominis* DHFR domain prevent substrate transfer.[7, 10] Furthermore, since the distance between the TS and DHFR domains is ~50-80 Å, the possibility of substrate channeling occuring via a major conformational change that brings the active sites close to one another is less plausible. An alternate possibility is that the transit of dihydrofolate from the TS to the DHFR site is governed by electrostatic substrate guidance, whereby charged residues on the surface of the enzyme generate an electric field that directs the substrate. Electrostatic substrate guidance has also been suggested as a mechanism by which acetylcholinesterase recruits substrate from solution.[6, 36, 38-41] The presence of substrate channeling in *L. major, P. falciparum*, and *T. gondii* and absence in *C.*

hominis may be due to the distinct host cell environments where each parasite has evolved to survive. The de novo folate biosynthesis pathway is present in both *T. gondii* and *P. falciparum*; however, the genes for folate biosynthesis are absent in the genome of *Cryptosporidium*. While *Toxoplasma* and *Plasmodium* can both carry out de novo synthesis and salvage folate, *Cryptosporidium* only has the ability to salvage folate from the host.[42, 43]

Several active site inhibitors selectively targeting the *T. gondii* TS and DHFR active sites over the human versions of the enzymes have been discovered, suggesting that the active sites of the parasite have a distinct architecture.[44-48] However, until now, the design of these inhibitors has largely relied on *in vitro* screening and homology modeling.[44, 47] Taking advantage of the unique structure of the *T. gondii* TS-DHFR active sites, as well as several nonconserved active site residues identified here, will enhance the structure-based development of selective inhibitors. The crystal structures presented here also pave the way for the design of allosteric inhibitors targeting non-active site regions of the enzyme, several of which have been described for other species of bifunctional TS-DHFR.[18, 49] For instance, the crossover helical region which is important is several aspects of enzyme catalysis could be targeted through virtual screening/molecular docking as well as small molecule screening. Recent findings have also indicated that the TS-TS interface of *T. gondii* TS-DHFR can serve as a target for the design of selective inhibitors.[50] Experiments analyzing these regions as potential targets for drug design are currently underway.

Supplementary Material

Refer to Web version on PubMed Central for supplementary material.

Acknowledgments

We thank the staff at the beam line station X25 and X29 at the National Synchrotron Light Source at Brookhaven National Laboratory for help during data collection. We thank Cindy Doan for performing bifunctional reaction of the S290G *C. hominis* TS-DHFR mutant and Ryan Pelto for his help in purifying methylene tetrahydrofolate. We also thank Dr. Kathleen Frey for helpful discussions regarding the structural studies.

Funding information: This work is supported by the NIH Grant AI 083146 (to K.S.A) and NIH Grant 5 T32 GM067543 (to M.J.L.).

Abbreviations

Å	Ångstrom
***B. bovis* (Bb)**	Babesia bovis
***C. hominis* (Ch)**	Cryptosporidium hominis
CH_2H_4F	5,10-methylene-5,6,7,8-tetrahydrofolate
DHFR	dihydrofolate reductase
DNA	deoxyribonucleic acid
dTMP	deoxythymidine monophosphate
DTT	dithiothreitol
dUMP	deoxyuridine monophosphate
E. coli	Escherichia coli
EDTA	ethylenediaminetetraacetic acid

H_2F	7,8-dihydrofolate
H_4F	(6R,S)-5,6,7,8-tetrahydrofolate
k_{burst}	burst rate
k_{cat}	turnover number
k_{chem}	rate of chemistry
K_m	Michaelis-Menten constant
***L. major* (Lm)**	Leishmania major
μM	micromolar
M	molar
mM	millimolar
MTX (methotrexate)	(2S)-2-[(4-{[(2,4-diaminopteridin-6-yl)methyl] (methyl)amino}phenyl)formamido]pentanedioic acid
NADPH	nicotinamide adenine dinucleotide phosphate, reduced
nm	nanometers
nM	nanomolar
***P. falciparum* (Pf)**	Plasmodium falciparum
PDDF	N^{10}-propargyl-5,8-dideazafolate
RMSD	root-mean-square deviation
s	second
***T. cruzi* (Tc)**	Trypanosoma cruzi
***T. gondii* (Tg)**	Toxoplasma gondii
TS	thymidylate synthase
V_{max}	maximum velocity
WT	wild-type

References

1. Sharma M, Chauhan PM. Dihydrofolate reductase as a therapeutic target for infectious diseases: opportunities and challenges. Future Med Chem. 2012; 4:1335–1365. [PubMed: 22800373]
2. Gangjee A, Jain HD, Kurup S. Recent advances in classical and non-classical antifolates as antitumor and antiopportunistic infection agents: part I. Anticancer Agents Med Chem. 2007; 7:524–542. [PubMed: 17896913]
3. Hardy LW, Finer-Moore JS, Montfort WR, Jones MO, Santi DV, Stroud RM. Atomic structure of thymidylate synthase: target for rational drug design. Science. 1987; 235:448–455. [PubMed: 3099389]
4. Schiffer CA, Clifton IJ, Davisson VJ, Santi DV, Stroud RM. Crystal structure of human thymidylate synthase: a structural mechanism for guiding substrates into the active site. Biochemistry. 1995; 34:16279–16287. [PubMed: 8845352]
5. Fierke CA, Johnson KA, Benkovic SJ. Construction and evaluation of the kinetic scheme associated with dihydrofolate reductase from Escherichia coli. Biochemistry. 1987; 26:4085–4092. [PubMed: 3307916]

6. Knighton DR, Kan CC, Howland E, Janson CA, Hostomska Z, Welsh KM, Matthews DA. Structure of and kinetic channelling in bifunctional dihydrofolate reductase-thymidylate synthase. Nat Struct Biol. 1994; 1:186–194. [PubMed: 7656037]
7. O'Neil RH, Lilien RH, Donald BR, Stroud RM, Anderson AC. Phylogenetic classification of protozoa based on the structure of the linker domain in the bifunctional enzyme, dihydrofolate reductase-thymidylate synthase. J Biol Chem. 2003; 278:52980–52987. [PubMed: 14555647]
8. Senkovich O, Schormann N, Chattopadhyay D. Structures of dihydrofolate reductasethymidylate synthase of Trypanosoma cruzi in the folate-free state and in complex with two antifolate drugs, trimetrexate and methotrexate. Acta Crystallogr D Biol Crystallogr. 2009; 65:704–716. [PubMed: 19564691]
9. Begley DW, Edwards TE, Raymond AC, Smith ER, Hartley RC, Abendroth J, Sankaran B, Lorimer DD, Myler PJ, Staker BL, Stewart LJ. Inhibitor-bound complexes of dihydrofolate reductase-thymidylate synthase from Babesia bovis. Acta Crystallogr Sect F Struct Biol Cryst Commun. 2011; 67:1070–1077.
10. Yuvaniyama J, Chitnumsub P, Kamchonwongpaisan S, Vanichtanankul J, Sirawaraporn W, Taylor P, Walkinshaw MD, Yuthavong Y. Insights into antifolate resistance from malarial DHFR-TS structures. Nat Struct Biol. 2003; 10:357–365. [PubMed: 12704428]
11. Anderson KS. Fundamental mechanisms of substrate channeling. Methods Enzymol. 1999; 308:111–145. [PubMed: 10507003]
12. Meek TD, Garvey EP, Santi DV. Purification and characterization of the bifunctional thymidylate synthetase-dihydrofolate reductase from methotrexate-resistant Leishmania tropica. Biochemistry. 1985; 24:678–686. [PubMed: 3922404]
13. Trujillo M, Duncan R, Santi DV. Construction of a homodimeric dihydrofolate reductase-thymidylate synthase bifunctional enzyme. Protein Eng. 1997; 10:567–573. [PubMed: 9215575]
14. Roos DS. Primary structure of the dihydrofolate reductase-thymidylate synthase gene from Toxoplasma gondii. J Biol Chem. 1993; 268:6269–6280. [PubMed: 8454599]
15. Brophy VH, Vasquez J, Nelson RG, Forney JR, Rosowsky A, Sibley CH. Identification of Cryptosporidium parvum dihydrofolate reductase inhibitors by complementation in Saccharomyces cerevisiae. Antimicrob Agents Chemother. 2000; 44:1019–1028. [PubMed: 10722506]
16. O'Neil RH, Lilien RH, Donald BR, Stroud RM, Anderson AC. The crystal structure of dihydrofolate reductase-thymidylate synthase from Cryptosporidium hominis reveals a novel architecture for the bifunctional enzyme. J Eukaryot Microbiol. 2003; 50(Suppl):555–556. [PubMed: 14736160]
17. Blakley RL. Crystalline Dihydropteroylglutamic Acid. Nature. 1960; 188:231–232.
18. Martucci WE, Udier-Blagovic M, Atreya C, Babatunde O, Vargo MA, Jorgensen WL, Anderson KS. Novel non-active site inhibitor of Cryptosporidium hominis TS-DHFR identified by a virtual screen. Bioorganic & medicinal chemistry letters. 2009; 19:418–423. [PubMed: 19059777]
19. Grumont R, Sirawaraporn W, Santi DV. Heterologous expression of the bifunctional thymidylate synthase-dihydrofolate reductase from Leishmania major. Biochemistry. 1988; 27:3776–3784. [PubMed: 2841973]
20. Matthews DA, Alden RA, Bolin JT, Freer ST, Hamlin R, Xuong N, Kraut J, Poe M, Williams M, Hoogsteen K. Dihydrofolate reductase: x-ray structure of the binary complex with methotrexate. Science. 1977; 197:452–455. [PubMed: 17920]
21. Atreya CE, Anderson KS. Kinetic characterization of bifunctional thymidylate synthasedihydrofolate reductase (TS-DHFR) from Cryptosporidium hominis: a paradigm shift for ts activity and channeling behavior. J Biol Chem. 2004; 279:18314–18322. [PubMed: 14966126]
22. Otwinowski Z, Minor W. Processing of X-ray Diffraction Data Collected in Oscillation Mode. Methods Enzymol Macromol Crystallogr. 1997; 276:307–326.
23. 4, C. C. P. The CCP4 suite: Programs for protein crystallography. Acta Crystallogr D Biol Crystallogr. 1994; 50:760–763. [PubMed: 15299374]
24. Strong M, Sawaya MR, Wang S, Phillips M, Cascio D, Eisenberg D. Toward the structural genomics of complexes: crystal structure of a PE/PPE protein complex from Mycobacterium tuberculosis. Proc Natl Acad Sci U S A. 2006; 103:8060–8065. [PubMed: 16690741]

25. Storoni LC, McCoy AJ, Read RJ. Likelihood-enhanced fast rotation functions. Acta Crystallogr D Biol Crystallogr. 2004; 60:432–438. [PubMed: 14993666]
26. Cody V, Pace J. Structural analysis of Pneumocystis carinii and human DHFR complexes with NADPH and a series of five potent 6-[5′-(omega-carboxyalkoxy)benzyl]pyrido[2,3-d]pyrimidine derivatives. Acta Crystallogr D Biol Crystallogr. 2011; 67:1–7. [PubMed: 21206056]
27. Emsley P, Cowtan K. Coot: model-building tools for molecular graphics. Acta Crystallogr D Biol Crystallogr. 2004; 60:2126–2132. [PubMed: 15572765]
28. DeLano, WL. The PyMol Molecular Graphics System. DeLano Scientific; Palo Alto, CA: 2002.
29. Sawaya MR, Kraut J. Loop and subdomain movements in the mechanism of Escherichia coli dihydrofolate reductase: crystallographic evidence. Biochemistry. 1997; 36:586–603. [PubMed: 9012674]
30. Doan LT, Martucci WE, Vargo MA, Atreya CE, Anderson KS. Nonconserved residues Ala287 and Ser290 of the Cryptosporidium hominis thymidylate synthase domain facilitate its rapid rate of catalysis. Biochemistry. 2007; 46:8379–8391. [PubMed: 17580969]
31. Johnson EF, Hinz W, Atreya CE, Maley F, Anderson KS. Mechanistic characterization of Toxoplasma gondii thymidylate synthase (TS-DHFR)-dihydrofolate reductase. Evidence for a TS intermediate and TS half-sites reactivity. J Biol Chem. 2002; 277:43126–43136. [PubMed: 12192007]
32. Liang PH, Anderson KS. Substrate channeling and domain-domain interactions in bifunctional thymidylate synthase-dihydrofolate reductase. Biochemistry. 1998; 37:12195–12205. [PubMed: 9724533]
33. Trujillo M, Donald RG, Roos DS, Greene PJ, Santi DV. Heterologous expression and characterization of the bifunctional dihydrofolate reductase-thymidylate synthase enzyme of Toxoplasma gondii. Biochemistry. 1996; 35:6366–6374. [PubMed: 8639582]
34. Dasgupta, T. Kinetic Characterization of the Malarial Drug Target, Thymidylate Synthase-Dihydrofolate Reductase: Implications for Novel Antifolate Design, Dissertation. Yale University School of Medicine; 2008. p. 40-48.
35. Martucci WE, Vargo MA, Anderson KS. Explaining an unusually fast parasitic enzyme: folate tail-binding residues dictate substrate positioning and catalysis in Cryptosporidium hominis thymidylate synthase. Biochemistry. 2008; 47:8902–8911. [PubMed: 18672899]
36. Atreya CE, Johnson EF, Williamson J, Chang SY, Liang PH, Anderson KS. Probing electrostatic channeling in protozoal bifunctional thymidylate synthase-dihydrofolate reductase using site-directed mutagenesis. J Biol Chem. 2003; 278:28901–28911. [PubMed: 12754260]
37. Dasgupta T, Anderson KS. Probing the role of parasite-specific, distant structural regions on communication and catalysis in the bifunctional thymidylate synthase-dihydrofolate reductase from Plasmodium falciparum. Biochemistry. 2008; 47:1336–1345. [PubMed: 18189414]
38. Elcock AH, Potter MJ, Matthews DA, Knighton DR, McCammon JA. Electrostatic channeling in the bifunctional enzyme dihydrofolate reductase-thymidylate synthase. J Mol Biol. 1996; 262:370–374. [PubMed: 8845002]
39. Franca TC, Medeiros AL, dos Santos EC, Santos-Filho OA, Figueroa-Villar JD. A complete model of the Plasmodium falciparum bifunctional enzyme dihydrofolate reductasethymidylate synthase. A model to design new antimalarials. J Braz Chem Soc. 2004; 15:450–454.
40. Sussman JL, Harel M, Frolow F, Oefner C, Goldman A, Toker L, Silman I. Atomic structure of acetylcholinesterase from Torpedo californica: a prototypic acetylcholine-binding protein. Science. 1991; 253:872–879. [PubMed: 1678899]
41. Tan RC, Truong TN, McCammon JA, Sussman JL. Acetylcholinesterase: electrostatic steering increases the rate of ligand binding. Biochemistry. 1993; 32:401–403. [PubMed: 8422348]
42. Hyde JE. Fine targeting of purine salvage in Cryptosporidium parasites. Trends in parasitology. 2008; 24:336–339. [PubMed: 18586557]
43. Hyde JE, Dittrich S, Wang P, Sims PF, de Crecy-Lagard V, Hanson AD. Plasmodium falciparum: a paradigm for alternative folate biosynthesis in diverse microorganisms? Trends in parasitology. 2008; 24:502–508. [PubMed: 18805734]
44. Pelphrey PM, Popov VM, Joska TM, Beierlein JM, Bolstad ES, Fillingham YA, Wright DL, Anderson AC. Highly efficient ligands for dihydrofolate reductase from Cryptosporidium hominis

and Toxoplasma gondii inspired by structural analysis. Journal of medicinal chemistry. 2007; 50:940–950. [PubMed: 17269758]

45. Gangjee A, Li W, Kisliuk RL, Cody V, Pace J, Piraino J, Makin J. Design, synthesis, and X-ray crystal structure of classical and nonclassical 2-amino-4-oxo-5-substituted-6-ethylthieno[2,3-d]pyrimidines as dual thymidylate synthase and dihydrofolate reductase inhibitors and as potential antitumor agents. Journal of medicinal chemistry. 2009; 52:4892–4902. [PubMed: 19719239]
46. Gangjee A, Jain HD, Queener SF, Kisliuk RL. The effect of 5-alkyl modification on the biological activity of pyrrolo[2,3-d]pyrimidine containing classical and nonclassical antifolates as inhibitors of dihydrofolate reductase and as antitumor and/or antiopportunistic infection agents. Journal of medicinal chemistry. 2008; 51:4589–4600. [PubMed: 18605720]
47. Gangjee A, Li W, Yang J, Kisliuk RL. Design, synthesis, and biological evaluation of classical and nonclassical 2-amino-4-oxo-5-substituted-6-methylpyrrolo[3,2-d]pyrimidines as dual thymidylate synthase and dihydrofolate reductase inhibitors. Journal of medicinal chemistry. 2008; 51:68–76. [PubMed: 18072727]
48. Sharma H, Yang J, Zaware N, Devambatla RKV, Queener SF, Anderson KS, Gangjee A. Discovery of potent and selective inhibitors of Toxoplasma gondii thymidylate synthasedihydrofolate reductase as a novel class of TS inhibitors for opportunistic infections. ACS Med Chem Lett. 2013 In press.
49. Atreya CE, Johnson EF, Irwin JJ, Dow A, Massimine KM, Coppens I, Stempliuk V, Beverley S, Joiner KA, Shoichet BK, Anderson KS. A molecular docking strategy identifies Eosin B as a non-active site inhibitor of protozoal bifunctional thymidylate synthasedihydrofolate reductase. J Biol Chem. 2003; 278:14092–14100. [PubMed: 12556445]
50. Landau MJ, Sharma H, Anderson KS. Selective peptide inhibitors of bifunctional thymidylate synthase-dihydrofolate reductase from Toxoplasma gondii provide insights into domain-domain communication and allosteric regulation. Protein science : a publication of the Protein Society. 2013
51. Pettersen EF, Goddard TD, Huang CC, Couch GS, Greenblatt DM, Meng EC, Ferrin TE. UCSF Chimera--a visualization system for exploratory research and analysis. Journal of computational chemistry. 2004; 25:1605–1612. [PubMed: 15264254]

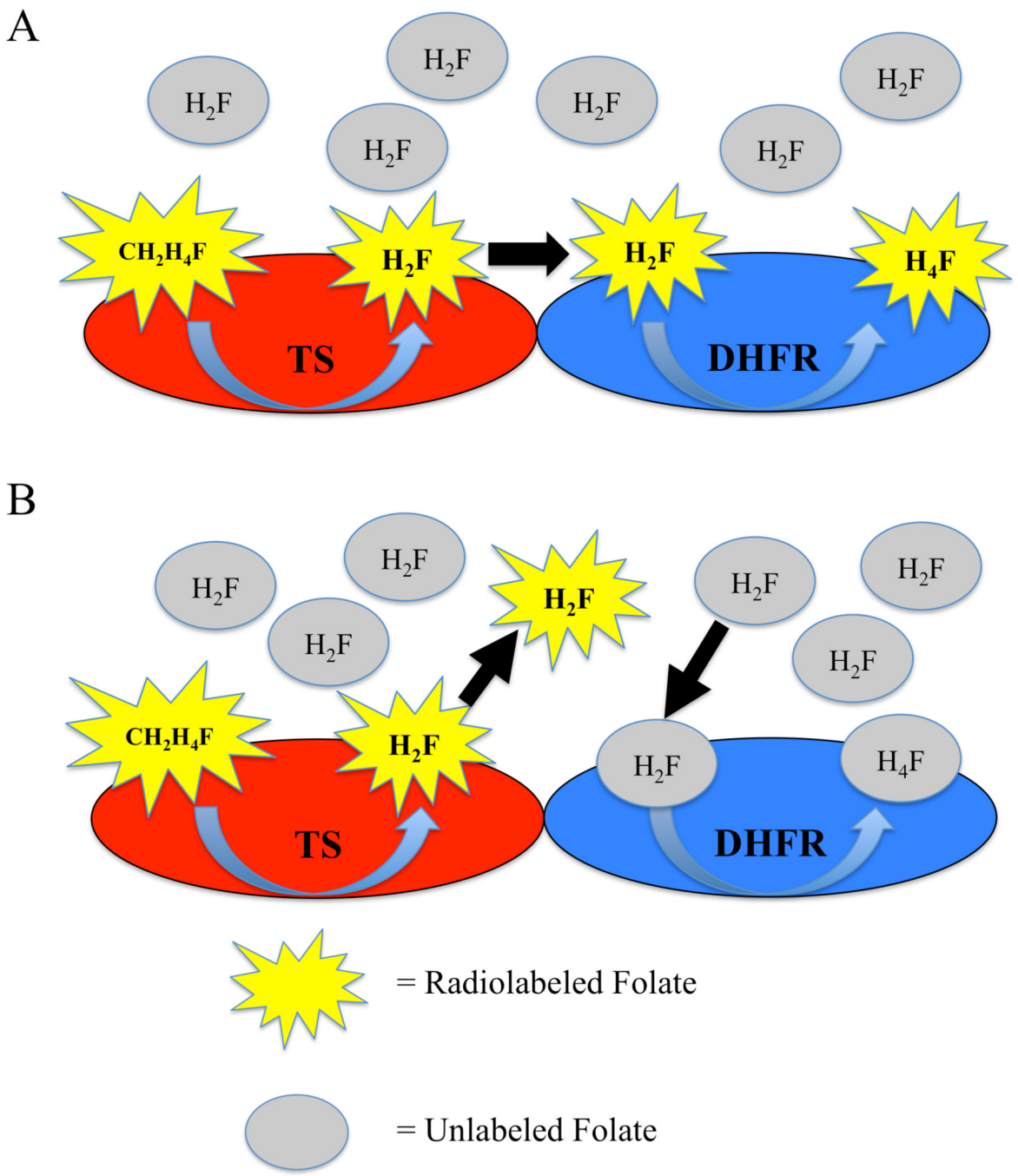

Scheme 1.

Diagram of the pulse-chase experiment for measuring H_2F channeling. We expected a channeling enzyme (**A**) to directly transfer the radiolabeled H_2F produced by the TS reaction to the DHFR domain without releasing it into solution, therefore only a small amount of the H_2F intermediate product would be observed. However, an enzyme unable to channel (**B**) would release radiolabeled H_2F into solution, where it would be outcompeted by an excess of unlabeled H_2F for substrate binding sites in the DHFR domain. In this scenario, a substantial buildup of radiolabeled H_2F in solution would be observed.

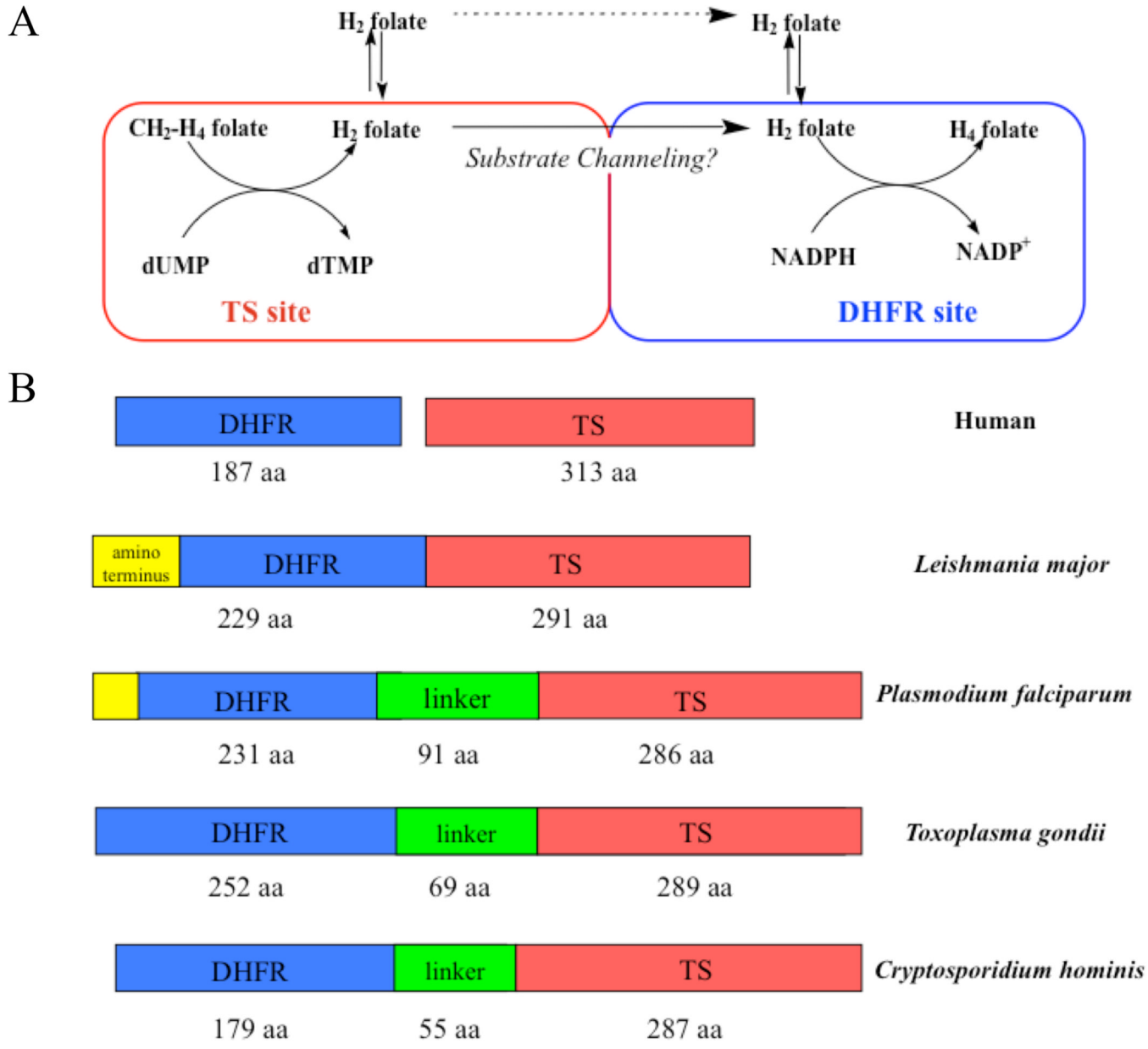

Figure 1.

(**A**) Schematic of reactions catalyzed by bifunctional TS-DHFR and substrate channeling. The TS reaction converts CH_2H_4F and dUMP to H_2F and dTMP, while the DHFR reaction converts H_2F to H_4F using NADPH as a cofactor. Substrate channeling occurs when H_2F is directly transferred from the TS to the DHFR without being released into solution by the TS and then bound from solution by DHFR. (**B**) Interspecies comparison of domains and linker regions in TS-DHFR.

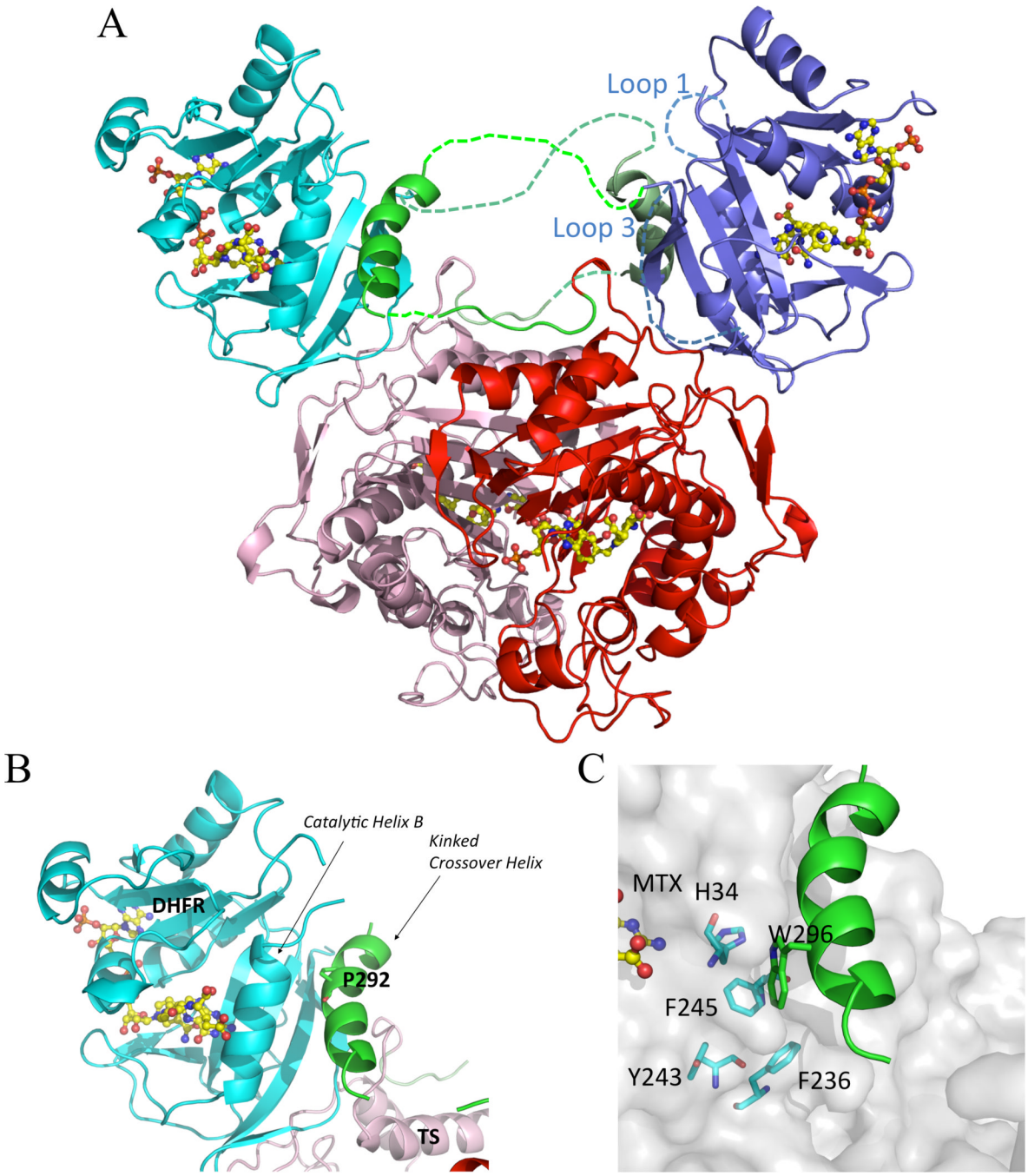

Figure 2.

(**A**) Overall crystal structure of the T. gondii TS-DHFR. The TS domains for each monomer are highlighted in red and pink, the DHFR domains are in blue and cyan, and the junctional regions are in two shades of green. The flexible surface loop 1 and 3 deletions are denoted by dashed lines (shown only for the DHFR domain in blue) (**B**) The kinked crossover helix and its position between the DHFR and the TS domains. (**C**) Key hydrophobic interactions between the crossover helix and the adjacent DHFR domain.

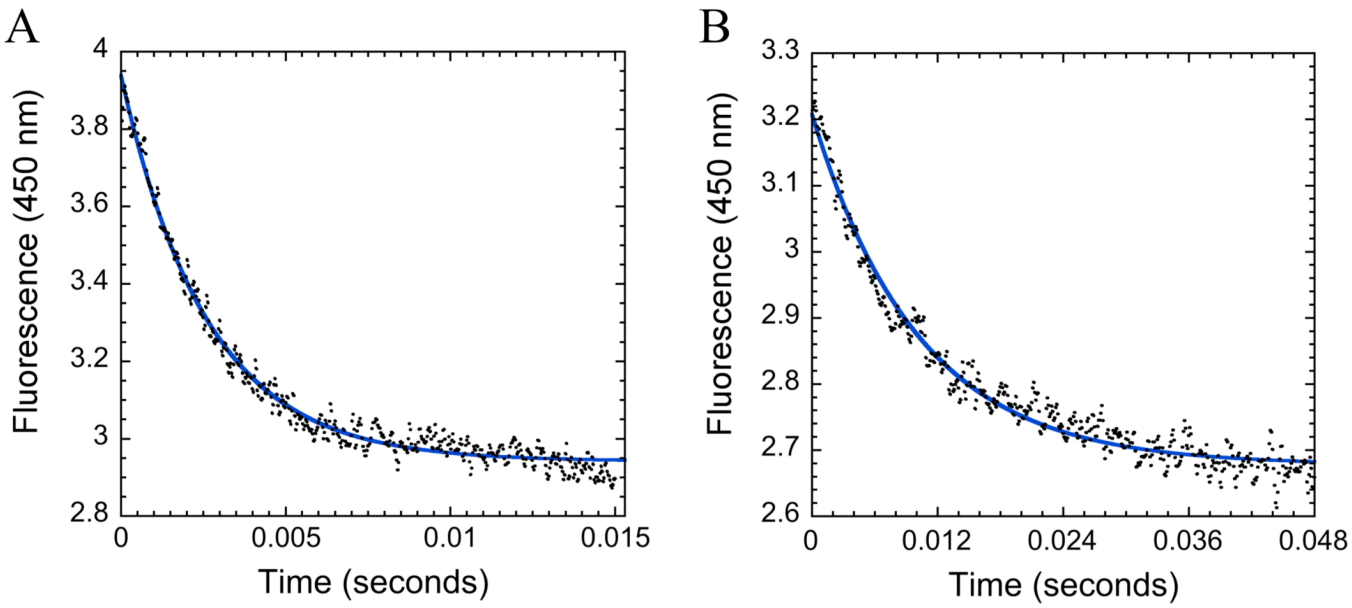

Figure 3.

Representative stopped-flow trace of DHFR catalysis of (**A**) WT and (**B**) W296A mutant as measured by NADPH fluorescence energy transfer at 450 nM. Enzyme (50 μM) was incubated with 250 μM of NADPH and mixed with 25 μM H_2F to examine the rate of chemistry (k_{chem}) in a single enzyme turnover. The data were to a single exponential for determine the rate of $NADP^+$ product formation.

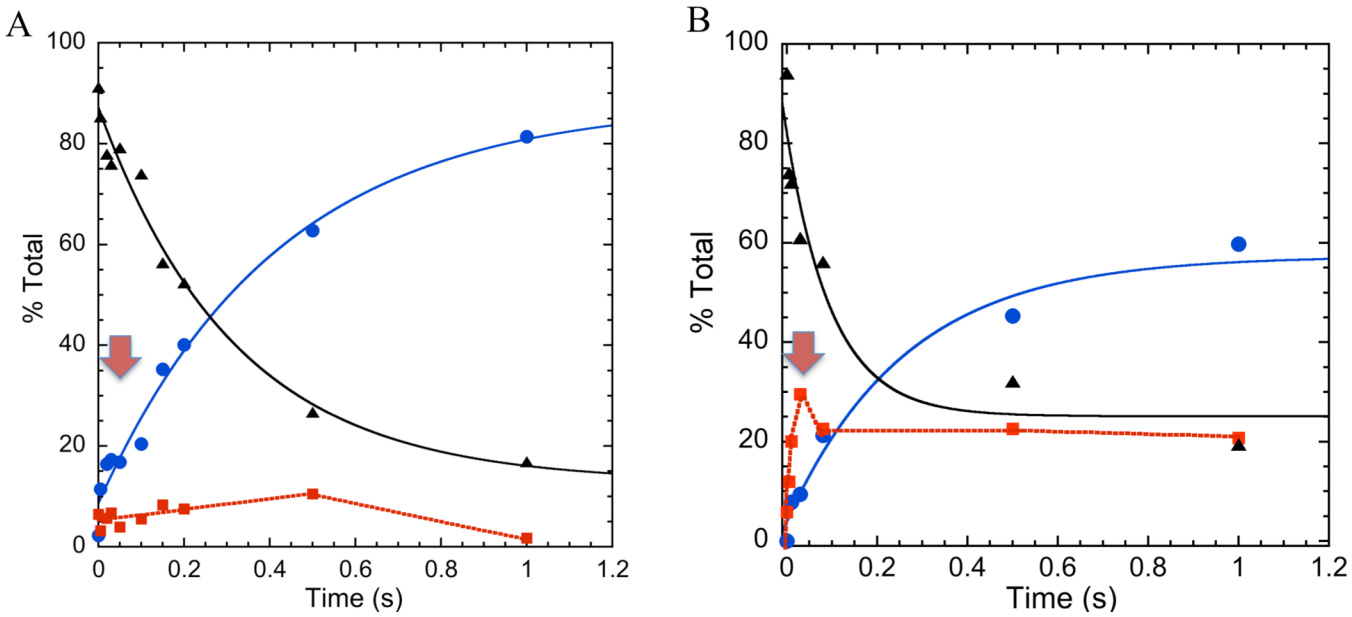

Figure 4.

Single turnover pulse-chase bifunctional reaction time courses for (**A**) *T. gondii* and (**B**) *C. hominis* TS-DHFR fit to a single exponential curve, showing the consumption of CH_2H_4F (black triangles) and production of H_4F (blue circles). Concentrations were normalized assuming the three substrates had a sum of 100% total content. Shown are representative time courses of experiments that were repeated in triplicate to confirm the reproducibility of the resultant rates. The peak of dihydrofolate buildup (red squares) is indicated by arrows.

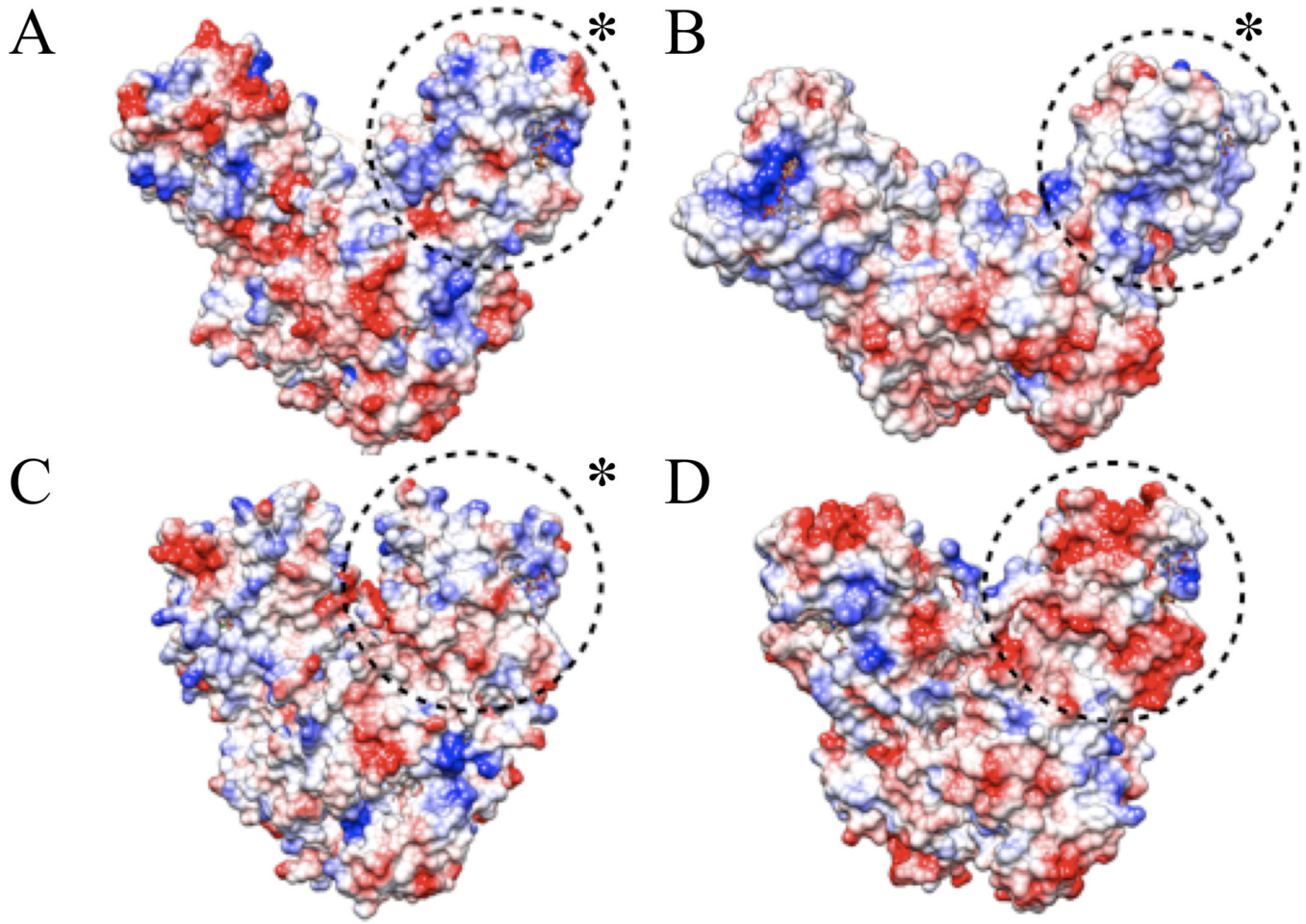

Figure 5.

Coulombic surface charge distributions of channeling and non-channeling TS-DHFRs. Figures of coloumbic charges were created by using Chimera[51] using default settings. Negative charges are colored red, and positive charges are colored blue. Pictured are the TS-DHFRs from (**A**) *T. gondii* (4EIL, loop truncated mutant), (**B**) *L. major*[6], (**C**) *P. falciparum* (PDB ID: 1J3I), and (**D**) *C. hominis* (PDB ID: 1QZF). The DHFR domain of each enzyme is circled. An asterisk (*) indicates a version of TS-DHFR capable of channeling.

Table 1

Crystallographic Statistics for Data Collection and Refinement

Molecule	**WT**	**Loop Truncation**
Space group	C121	P1
Dimers/AU	1	4
Unit cell dimensions		
a (Å), α(°)	185.9 , 90	53.8, 90.1
b (Å), β(°)	143, 90	144.4, 90.0
c (Å), ξ(°)	59.8, 90	177.6, 90.4
Resolution (Å)	50-3.56 (3.63-3.56)	50-2.2 (2.24-2.2)
Wavelength (Å)	1.1	1.1
Completeness (%)	94.5 (90.3)	98.0 (96.5)
Redundancy	3.6	6.6
Total number of reflections	1745090	4910878
Unique reflections	17754	265904
R_{sym}	0.240 (0.768)	0.152 (0.718)
I/σ	5.42 (2.15)	10.98 (2.14)
rmsd bond length, Å	0.010	0.0093
rmsd bond angle, °	1.568	1.490
R_{cryst} %	34.66	22.44
R_{free} %	39.86	24.55
Protein statistics from Ramachandran plot		
Residues in favored regions	81.2%	96.4%
Residues in allowed regions	12.0%	2.8%
Outliers	6.8%	0.75%
PDB ID Code	4ECK	4EIL

The values in parentheses are for the highest-resolution shell. R_{sym} is $\Sigma|Ij\text{-}I|/\Sigma I$, where Ij is the intensity of an individual reflection, and I is the mean intensity for multiple recorded reflections. R_{cryst} is $2\ \Sigma\ |F_O - F_C|/\ \Sigma F_O$, where F_O is an observed amplitude and F_C a calculated amplitude; R_{free} is the same statistic calculated over a subset, 5%, of the data that have not been used for refinement.

Table 2

Summary of Protein Ligand and Protein-Protein Interactions

Protein Ligand and Protein-Protein Interactions*	Residues
DHFR domain - TS domain (electrostatic)	Arg173 - Pro568
	Ser194/Asn195/Ala191 - Arg569
	Ile232 - Gly321
	Thr235 - Phe571
	Ser237 - Gln363
	Asp244 - Pro570
DHFR domain - TS domain (hydrophobic)	Arg176 - Val596
	Ile192/Ile232 - Glu567
	Arg228 - His316
	Pro229 - Glu567/His316
	Ile230 - His318
	Phe231/Met 297 - Phe319
	Pro242 - Ile573/Val596
DHFR - crossover helix (electrostatic)	Lys33 - Glu300
	Glu249 - Ser286
DHFR - crossover helix (hydrophobic)	His34/Phe236/Tyr243/Phe245 - Trp296
	Tyr170 - Ile290/Val293
	Phe231 - Val293/Leu294
	Phe231 - Met297
	Phe319 - Ile290/Leu294
dUMP - TS domain	Arg344, Arg469, Arg470, Cys489, Gln509, Arg510, Ser511, Cys512, Asp513, Asn521, His551, Tyr553
PDDF - TS domain	Ile402, Asp513, Leu516, Phe520, Arg603, Met608
MTX - DHFR domain	Ala10, Asp31, Phe32, Phe35, Met87, Phe91, Arg97
NADPH - DHFR domain	Ala10, Ile17, Ile19, Gly22, Arg81, Thr83, Val102, Ser103, Gly153, Ala154

* Pairs of residues with interatomic distances within 3.5Å are considered to be interacting with one another. For hydrophobic interactions, distances within 5Å are considered.

Table 3

DHFR Kinetic Constants. [a]

Enzyme	Km H2F (μM)	K_m NADPH (μM)	kcat(s^{-1})	kchem (s^{-1})
T. gondii WT	0.15 ± 0.03	2.5 ± 0.2	3.3 ± 0.4	407 ± 36
Tg P292A	0.92 ± 0.14	3.7 ± 1.1	3.0 ± 0.1	752 ± 87
Tg W296A	17.2 ± 2.0	10.1 ± 1.8	3.7 ± 0.2	95.7 ± 4.1
Tg Helix Deletion	6.3 ± 1.0	16.4 ± 2.7	4.2 ± 0.6	86.4 ± 2.4
Tg Loop Truncation	0.26 ± 0.06	5.1± 0.7	3.4 ± 0.2	303 ± 2

[a] Errors in the steady state turnover rate (k_{cat}) and Michaelis constant (K_m) result from standard error of parameters generated from the curve-fitting program KaleidaGraph. Errors in the single turnover rate of DHFR chemistry (k_{chem}) result from averaging resultant fits from triplicate measurements of stopped-flow fluorescence traces.

Table 4

TS kinetic constants.[a]

Enzyme	K_m CH_2H_4F (μM)	K_m dUMP (μM)	kcat (s^{-1})	k_{burst} (s^{-1})	Bifunctional rate (s^{-1})
T. gondii WT	9.5 ± 1.7	0.54 ± 0.13	0.84 ± 0.04	202.8 ± 9.4	3.1 ± 0.5
TG W296A	10.5 ± 3.3	2.6 ± 0.3	0.51 ± 0.01	106.7 ± 2.8	2.9 ± 0.6
TG Helix Deletion	3.6 ± 0.5	2.8 ± 0.4	0.90 ± 0.02	93.5 ± 3.3	3.6 ± 0.6
TG Loop Truncation	14.3 ± 1.6	0.50 ± 0.09	1.07 ± 0.07	256.2 ± 30.3	4.9 ± 0.8

[a]Errors in k_{cat}, K_m, and the bifunctional single turnover rate result from standard error of parameters generated from the curve-fitting program KaleidaGraph. Errors in the rate of the TS burst reaction (k_{burst}) result from averaging the resultant fits from triplicate measurements of stopped-flow absorbance traces.